Artificial Neural Network Control Applied to a Photovoltaic-Battery Microgrid System

Chabakata Mahamat, Jessica Bechet, Laurent Linguet

acrt AI, Computer Science and Robotics Technology

IntechOpen Journals

RESEARCH PAPER

Artificial Neural Network Control Applied to a Photovoltaic-Battery Microgrid System

Chabakata Mahamat*, Jessica Bechet and Laurent Linguet

University of French Guiana, UMR Espace-Dev, Cayenne, French Guiana
*Corresponding author. E-mail: chabakata.mahamat@univ-guyane.fr

Citation
Chabakata Mahamat, Jessica Bechet and Laurent Linguet (2024), Artificial Neural Network Control Applied to a Photovoltaic-Battery Microgrid System. *AI, Computer Science and Robotics Technology* 3(1), 1–20.

DOI
https://doi.org/10.5772/acrt.34

Received: 20 October 2023
Accepted: 12 April 2024
Published: 17 May 2024

Abstract

This paper deals with artificial neural network (ANN) applied to control a standalone microgrid in French Guiana. ANN is an artificial intelligence technique used to control non-linear and complex systems. ANN associated with the Levenberg–Marquardt (LM) algorithm has many advantages, such as rapid decision-making and improved system transients. Therefore, this technique should be adapted for the control of photovoltaic (PV) systems in the tropical climate of French Guiana with high variation in irradiance. The microgrid is composed of a PV source and a storage battery to supply an isolated building which is modeled by a DC load. The PV source is controlled by an ANN-based MPPT (Maximum Power Point Tracking) controller. To validate our ANN-MPPT, we compared it with one of the very popular MPPT algorithms, which is the P&O-MPPT algorithm. The comparison results show that our ANN-MPPT works well because it can find the maximum power point quickly. In the case of battery control, we tested two feed-forward backpropagation neural network (FFBNN) configurations called method1 and method2 associated with the Levenberg–Marquardt (LM) algorithm. We varied the number of hidden layers in each of these two FFBNN configurations to obtain the optimal number of hidden layers for each configuration which optimizes battery control. Method1 is chosen because it is better than method2, in a sense that it respects the maximum amplitude of the battery current for our application and improves the transient regimes of this current. This best configuration (method1) is

then tested with two other learning algorithms for comparison: Bayesian regularization (BR) and scaled conjugate gradient (SCG) methods. The system performance with LM algorithm is better than SCG and BR algorithms. LM algorithm improves the performance of the system in transient regimes while the results obtained with the SGG and BR algorithms are similar. Then, we focused on the advantage of using ANN control compared to the conventional proportional integral control (PI control). The comparison results showed that ANN control associated with the LM algorithm (ANN-LM) made it possible to reduce battery current peaks by 26% in transient regimes compared to conventional PI control. Finally, we present and discuss the results of our simulation obtained with the MATLAB Simulink software.

Keywords: PV-battery system, microgrid, ANN control, ANN based MPPT

1. Introduction

The energy sector faces a steady increase in global energy consumption, mainly due to demographic evolution. The largest raise in energy demand will take place in developing countries where the proportion of global energy consumption is expected to increase from 46 to 58% between 2004 and 2030 [1]. Even though in 2020 the global energy consumption decreased by 5.9% compared to 2019 due to COVID-19 pandemic, the demand for renewable energy increased by nearly 1.5% [2]. The energy sector is therefore faced with challenges related to the integration of renewable energies. Solar energy is one of the fastest growing energies and photovoltaic (PV) technology is widely installed in residential buildings [3].

Microgrids based on PV technology, with a robust control, can reduce power fluctuations by providing output power smoothing, ensuring service continuity, and stabilizing the grid [4, 5].

French Guiana is a French overseas territory, located in Latin America and has a tropical climate, where solar energy is one of the most widespread renewable energies [6, 7]. But equipment is imported from Europe and is therefore not adapted to the tropical climate of French Guiana. So, this equipment degrades quickly because of the severity of this climate. In addition, if the system is poorly controlled, their degradation can accelerate due to the bad behavior of the system in transient regimes which generates current peaks.

To limit these negative effects on the battery, we propose to use artificial neural networks (ANN) which are artificial intelligence techniques used to control nonlinear and complex systems [8]. Indeed, many scholars have used ANN in several different ways [8–14]. But to the best of our knowledge, no study has been

done using ANN controllers to control the battery to better respect its technological constraints and thus improve its lifetime in a tropical climate context.

Using these innovative techniques in this domain permits improvement in the transient regimes of the battery current in order to improve its lifetime and therefore reduce the operating cost of the system.

This paper is organized into the following sections: Section 2 presents the methodology; Section 3 presents the results and discussion. Finally, Section 4 presents the conclusion.

2. *Methodology*

2.1. Description of the system

The block diagram of the studied system is presented in Figure 1. The system is composed of two parts: a source part consisting of a photovoltaic generator (PVG) which supplies the isolated building which is modeled by a DC load through a DC/DC boost converter; and a storage part consisting of a battery connected to the *DC* load through a reversible DC/DC converter.

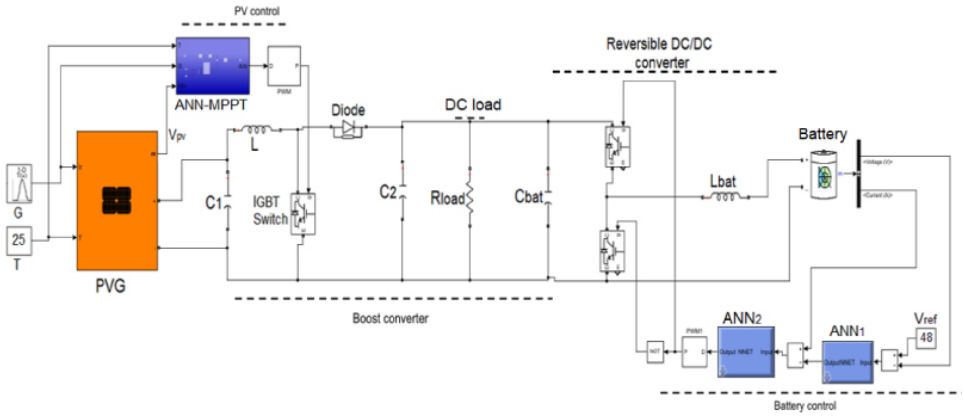

Figure 1. Block diagram of the system.

As shown in Figure 1, the source part is controlled by an ANN-MPPT (ANN-based Maximum Power Point Tracking) block. As for the battery, it is controlled by two ANN controllers (ANN1 and ANN2). We detail these controls in the following section.

2.1.1. ANN presentation

As previously mentioned, artificial neural networks (ANN) are artificial intelligence techniques used to control non-linear and complex systems. They have various

merits, such as, excellent approximation of nonlinear function, fast decision making, no restriction on the normality etc. For each ANN model, there are several key configurations such as the number of hidden layers, the activation function etc. [10, 14].

Each artificial neuron is an elementary processor which receives a variable number of inputs from upstream neurons. Each input is associated with a weight (b_i) representing the strength of the connection. Each elementary processor has a single output, which then branches out to supply a variable number of downstream neurons. Each connection is associated with a weight [10]. The diagram of a formal neuron is shown in Figure 2. The principal equation of an ANN describes in

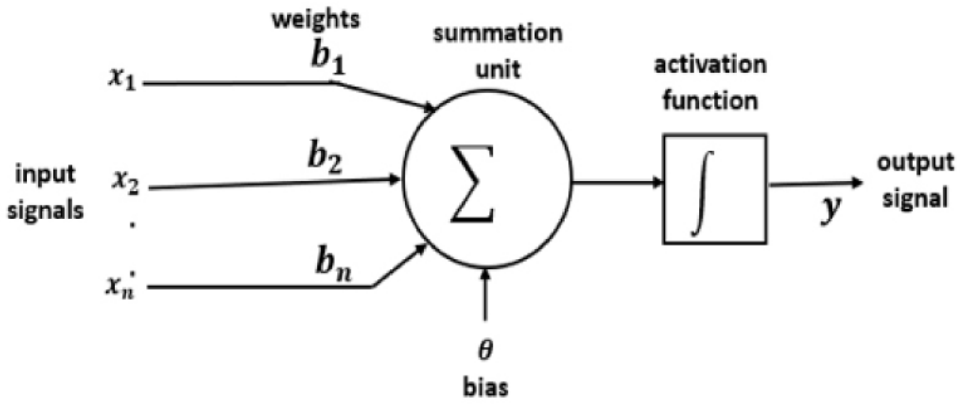

Figure 2. Diagram of a formal neuron.

Figure 2 is given in (1).

$$f\left(\sum_{i=1}^{n} b_i \cdot x_i + \theta\right) = y \tag{1}$$

Where: x_i (i = 1, 2 ... n), inputs signals; y, output; b_i (i = 1, 2 ... n), weights; f, activation function; θ, bias.

2.1.2. ANN architecture and learning algorithm choice

There are several neural network architectures and learning algorithms. A very popular and efficient one would be the backpropagation learning algorithm [10, 11]. According to [10], Levenberg–Marquardt method (LM) is based on the non-linear least squares technique and the Gauss–Newton algorithm with restricted neighborhood. It is a standard algorithm for the quadratic error optimization due to its fast convergence and robustness properties [10]. Still according to the same author, LM algorithm permits lower cost of calculations and the fast guarantee of convergence to a minimum.

According to [15], LM algorithm would be faster than others training algorithm like Bayesian regularization and scaled conjugate gradient methods. It is recommended for training the network.

For all these reasons, we choose, both for source part control and battery control, a neural network of the feed-forward backpropagation type, by using Matlab Software, with the training function TRAINLM (Levenberg-Marquardt Backpropagation) and "logsig, tansig and purelin" as activation functions for input layer, hidden layer, and output layer respectively.

2.2. Source part control: PV control

As previously mentioned, the source part is controlled by an ANN-based MPPT presented in [10] and [16]. Its principle is illustrated in Figure 3 and its simulation scheme is shown in Figure 5.

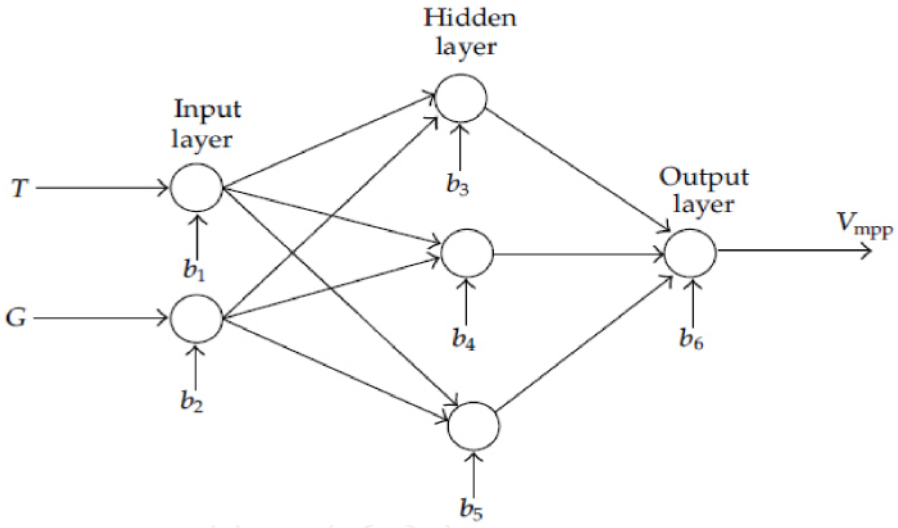

Figure 3. Algorithm of ANN-MPPT method [16].

The role of ANN (see Figure 3) is to deliver the optimal voltage V_{mpp} (which gives the maximum power) from the climatic data at the input of the PVG: irradiance (G) and temperature (T).

In this case, G and T are two input variables and V_{mpp} is the output variable of this first ANN-MPPT controller.

2.2.1. Dataset of ANN controllers

To set up ANN controllers, it is necessary to obtain data as input and output variables to train the neural network. For this, we randomly generated the data

using a MATLAB program by considering the following equations [16, 17]:

$$G = (G_{max} - G_{min}) \cdot \text{rand} + G_{min} \quad (2)$$

$$T = (T_{max} - T_{min}) \cdot \text{rand} + T_{min} \quad (3)$$

$$V_{mpp} = V_m + \beta(T - T_s) \quad (4)$$

$$I_{mpp} = I_m \cdot \left(\frac{G}{G_s}\right) \cdot (1 + \alpha)(T - T_s) \quad (5)$$

where: G, irradiance variation; G_s, standard irradiance (G_s = 1000 W/m²); G_{max}, maximum irradiance (we choose G_{max} = 1200 W/m²); G_{min}, minimum irradiance (G_{min} = 0 W/m²); T, temperature variation; T_s, standard temperature; T_{max}, maximum temperature (T_{max} = 36 °C); T_{min}, minimum temperature (T_{min} = 18 °C) α, current temperature coefficient; β, voltage temperature coefficient;

V_m, maximum voltage of the considered panel (from datasheet); I_m, maximum current of the considered panel (from datasheet); rand, random function of the MATLAB.

Note that the choice of minimum and maximum parameters are made according to the realities of the field of study (French Guiana).

So, by considering Equations (2)–(5) and using "for loop" in MATLAB, it is possible to build the needed data to train our ANN models. For this, we arbitrarily chose to build 1500 samples.

Afterwards, as previously announced, we chose the error backpropagation method with LM algorithm to train our ANN models as in [10] and [16]. Moreover, three hidden-layer-neural network is used to reach V_{mpp} as shown in Figure 3 [16]. The same number of hidden layers is used for the second ANN controller (ANN-reg).

Figure 4 shows the regression curve of the training of the ANN-MPPT model carried out in this work. It can be seen that the regression (R) is equal to one (R = 1) indicating that our ANN-MPPT model is 100% successfully trained.

The first ANN controller (ANN-MPPT) having given the reference voltage V_{mpp}, this voltage is then used by a second ANN controller (ANN-reg) which compares it to the input voltage of the boost converter (V_{pv}) to deliver the optimal current I_{mpp} (also called current under MPPT). Then, the duty cycle for controlling the boost is obtained, after passing through the PWM (pulse width modulation) block.

Figure 5 shows the simulation scheme of the source part control (PV control).

Our ANN-based MPPT method is similar to those presented in [10] and [16] but with a slight difference. Indeed, in [10], the authors consider a single ANN controller with three inputs (V_{pv}, I_{pv} and P_{pv}) and one output (duty cycle) while our method

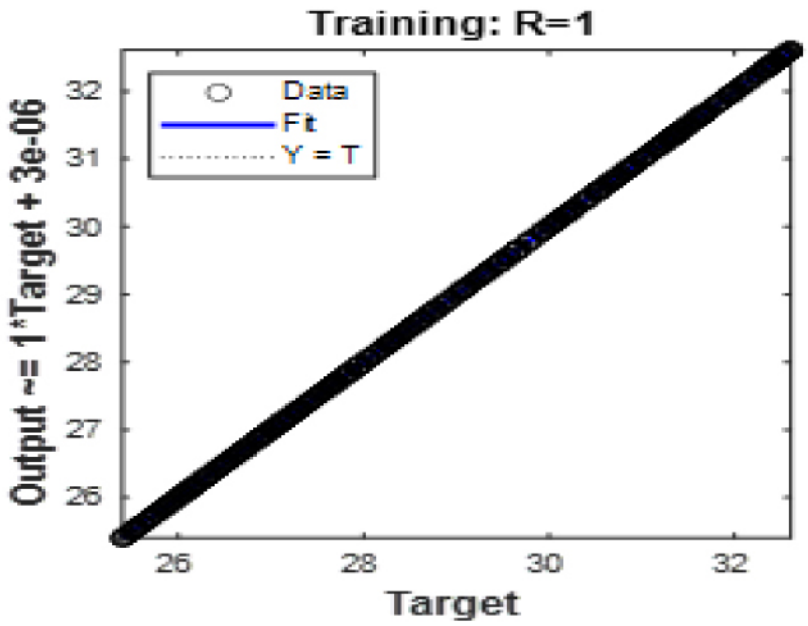

Figure 4. Regression curve of the trained ANN-MPPT model.

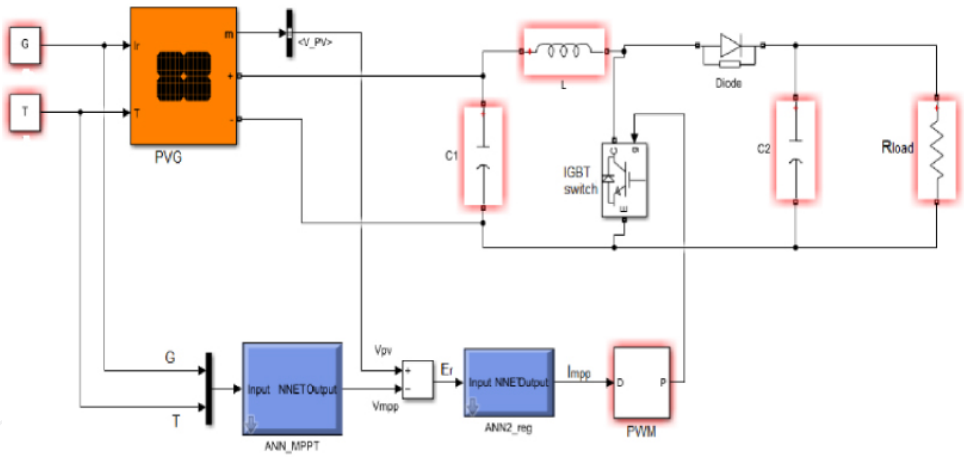

Figure 5. Source part control (PV control).

presents two ANN controllers: the first has two inputs (G, T) and one output (V_{mpp}) and the second has one input (Er: the comparison error between V_{mpp} and V_{pv}) and one output (I_{mpp}). As for the method presented in [16], it presents an ANN controller which has the same inputs (G, T) and output as our first ANN controller and a proportional and integral (PI) controller which plays the role of our second ANN controller. So, we replaced PI controller with an ANN controller to have 100% ANN control.

The result of the source part control is presented in Section 3 (result and discussion).

2.3. Battery control

The battery control contains two nested loops:

A voltage loop which compares the reference voltage (V_{dc}^* = 48 V) and the measured voltage of the DC load (V_{dc}) to deliver a battery reference current (I_{bat}^*) and a current loop which uses I_{bat}^* to control the battery current (I_{bat}).

The block diagram of the proposed battery ANN control is illustrated in Figure 6.

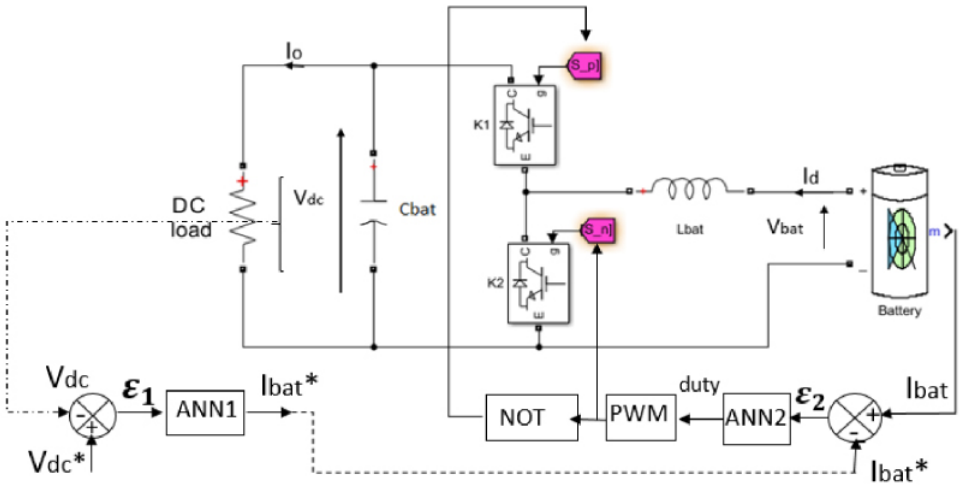

Figure 6. Block diagram of the proposed battery control.

To set up ANN controllers for controlling the battery, we generated the data (1500 samples) by using a MATLAB program and the parameters of the battery which are indicated in Table 3.

We tested different configurations of this ANN model according to the number of neurons in the hidden layer to choose the best configuration for the most efficient ANN model. Indeed, the role of the input layer is to transfer the input values corresponding to the input variables (input data) to the next layer called the hidden layer [10]. Therefore, the number of input layers depends on the number of input data to be processed. The number of the output layers also depends on the number of output data.

To choose the number of input layers, we asked ourselves if the comparator should be in or outside the ANN controller as the number of input data differs

depending on whether the comparator is included in the ANN or not. Hence our two methods: method1 and method2.

2.3.1. Method1: comparator outside the ANN controller

In this configuration method, we consider the comparator to be outside the ANN controller (Cf. Figure 6). In this case, the ANN controller input is the comparison error (ε_i). So we only need one input layer and one output layer because we have only one input (ε_i; i = 1, 2) and one output per ANN controller ($x = I_{bat}^*$, duty) as shown in Figure 6. But the number of neurons in the hidden layer can vary. Where ε_i is the comparison error.

Table 1 shows the performance of ANN according to the number of neurons in the hidden layer (for method1).

Table 1. Performance of ANN as a function of number of neurons in the hidden layer (method1).

ANN1		ANN2	
Hidden layer number	**MSE (%)**	**Hidden layer number**	**MSE (%)**
2	26.5529	2	0.026072
3	22.659	3	0.02579
4	22.4424	4	0.015102
5	22.3476	5	0.024541
6	22.3608	6	0.014644
7	22.1468	7	0.014855
8	22.2094	8	0.014914
9	22.0856	9	0.014512
10	22.4147	10	0.014568

As shown in Table 1, the best configurations are those for which the number of hidden layers is equal to nine for the two ANN controllers (ANN1 & ANN2). Indeed, these configurations have the lowest mean square error (*mse* = 22.0856% for ANN1 and *mse* = 0.014512% for ANN2) and therefore the best performance.

2.3.2. Method2: comparator inside of the ANN controller

Figure 7 shows the principle of the method2.

As shown in Figure 7, in configuration method2, instead of the input of the ANN controller being a comparison error between the measured quantity and its reference (between I_{bat}^* and I_{bat} for example), the comparator is included in the ANN controller. So, each ANN controller uses two input quantities, i.e. the reference quantity and the measured quantity, and is trained to provide the desired signal.

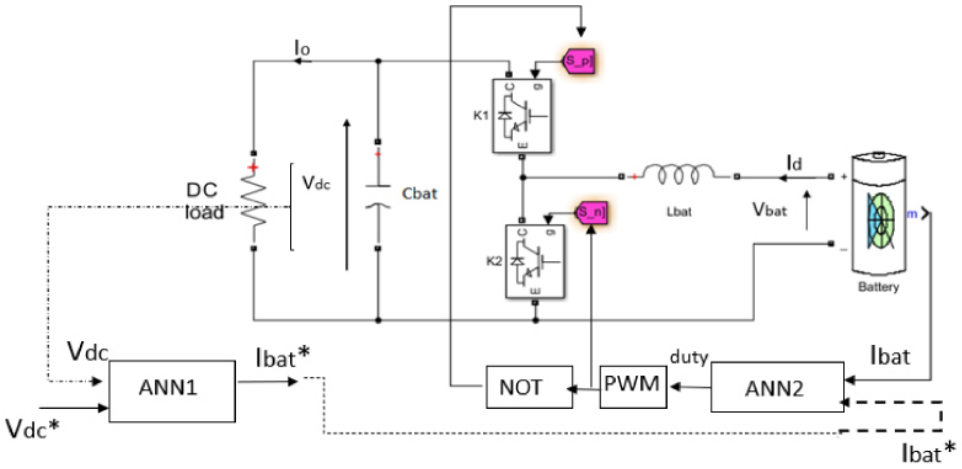

Figure 7. Configuration method2 of ANN controllers.

In this case, two input layers and one output layer are required as we have two input data (V_{dc} and V_{dc}^* for ANN1; I_{bat} and I_{bat}^* for ANN2) and one output per ANN controller ($x = I_{bat}^*$, duty) as shown in Figure 7. But the number of neurons in the hidden layer can vary.

Table 2 shows the performance of ANN according to the number of neurons in the hidden layer (for method2).

Table 2. Performance of ANN as a function of number of neurons in the hidden layer (method2).

ANN1		ANN2	
Hidden layer number	**MSE (%)**	**Hidden layer number**	**MSE (%)**
2	26.2949	2	0.010255
3	22.5856	3	0.01015
4	22.8456	4	0.0098326
5	22.377	5	0.0097088
6	22.1368	6	0.0097896
7	22.4019	7	0.009624
8	22.1476	8	0.0098795
9	22.124	9	0.0097267
10	22.5518	10	0.0097808

Table 2 indicates that the best configurations are those for which the number of hidden layers is equal to nine and seven for ANN1 and ANN2 respectively with *mse* = 22.1229% for ANN1 and *mse* = 0.0096748% for ANN2.

Each ANN model is trained with 1500 data samples for both method1 and method2. Thus, after having trained the models, we use the MATLAB command "gensim" to generate the Simulink toolbox of the ANN controller which is then used in the Simulink model of the simulation.

To choose between the two methods, we superposed the simulation result obtained by the two methods in Figure 10. Looking at Figure 10, both methods work but method1 is better than method2. Indeed, not only does the amplitude of the battery current obtained with method1 correspond exactly to the maximum amplitude of our application (I_{bat_max} = 8. 88 A) but in addition, method1 presents an overshoot current in transient regime lower than in the case of method2 (30.06 A vs 37.37 A). This is the reason why method1 was chosen in this study.

Figure 8 shows the model of the ANN controllers thus configured (with method1).

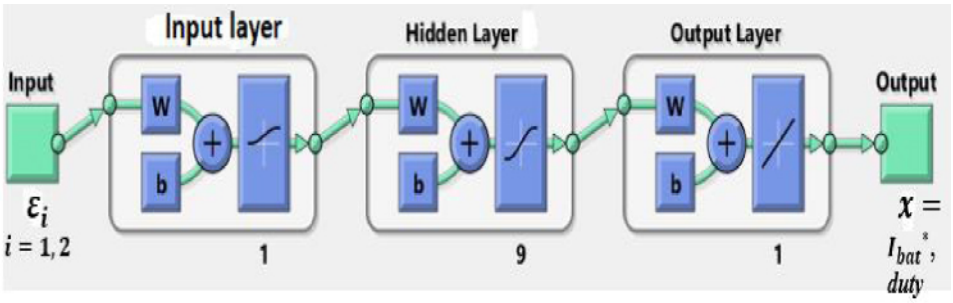

Figure 8. Configured ANN network (method1).

Our method of synthesizing an ANN controller is summarized in Figure 9.

To justify the choice of the LM algorithm, starting from the same optimal number of hidden layers (nine) presented in Table 1 and considering the same activation functions ("logsig, tansig and purlin"), we have implemented the model of method1 with two other training functions: Bayesian regularization (BR) and scaled conjugate gradient (SCG) methods. The result presented in the following section confirms that our choice of the LM algorithm is judicious in terms of improving transient regimes.

Moreover, to validate our ANN control, we compared it with the conventional Proportional Integral (PI) control whose parameters (of PI) are calculated in [18].

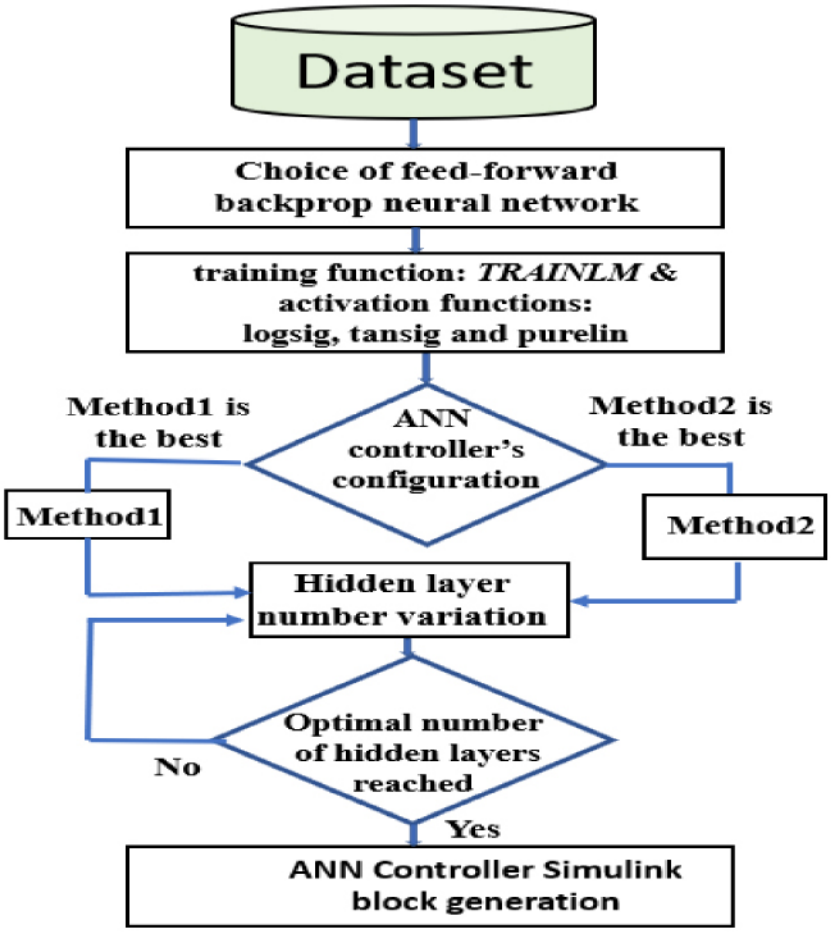

Figure 9. The steps of synthesis of our ANN controllers.

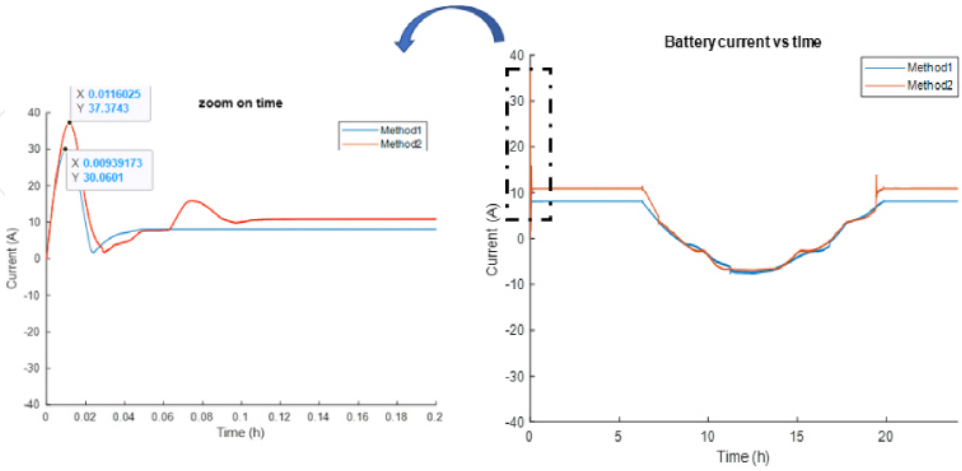

Figure 10. Battery current for comparison of the methods (method1 vs method2).

3. Simulation results and discussion

The simulation is carried out with the parameters indicated in Table 3. For more information on these parameters, see [18].

Table 3. Parameters of the simulation.

Source part		
Symbol	**Parameter**	**Value**
1STH-215-P	PV model	
I_{sc}	Short circuit current	7.84 A
V_{oc}	Open circuit voltage	36.3 V
$P_{\max}$	Maximum power	213.15
V_{mpp}	Maximum voltage	29 V
I_{mpp}	Maximum current	7. 35
N_s	Number of cells in series	60
R_s	Series resistances	0.39383 Ω
R_{sh}	Shunt resistance	313.3991 Ω
n	Cell ideality factor	0.98117
α	Current temperature coefficient	0.102
β	Voltage temperature coefficient	**−0.36099**
N_p	Number of parallel string	5
N_s'	Number of strings in series	1
PPVG_max	Maximum power of the PVG	1.066 kW
L	Inductance of the boost converter	5 mH
C1	Input capacitor of the boost	3300 µF
C2	Output capacitor of the boost	330 µF
f_{sw}	Switching frequency of the boost	10 kHz
	DC load	
R_{load}	Load resistance	5.2 Ω
V_{dc}	Voltage of the DC load	48 V
P_{load}	Power consumed by the DC load	426 W
	Storage part	
Symbol	Parameter	Value
Lithium-ion	Type of the battery	
dt	The need autonomy of the battery	2.3 h
$I_{\mathrm{bat\_max}}$	Maximum battery current	8.88 A
V_{bat}	Input battery voltage	
Q	Capacity of the battery	17.76 h
SOC	Initial state of charge	45%
L_{bat}	Battery side inductance	5.2 mH
C_{bat}	Battery side capacitor	400 µF
f_{sw}	Switching frequency of the RDC	10 kHz

3.1. Study area

We have chosen the municipality of Saül which is an isolated municipality in a sense that it is not connected to the coastal electricity distribution network of French Guiana. To test the control, we chose the sunniest day of the year 2020 (11/09/2020) for this study area.

3.2. Simulation results

Simulation results are shown in the following Figures 11–16. The irradiance (Cf. Figure 11) is estimated (every one hour) by a computer program developed by us [19]. To simplify, we have implemented in MATLAB the daily irradiance profile in seconds instead of hours. This is why the time-axis is in second.

3.3. Discussions

Figure 11, Figure 12 and Figure 13 show the variations of irradiance (G) PV power (P_{pv}) and PV current (I_{pv}) respectively. We can see in Figure 12 and Figure 13 that P_{pv} and I_{pv} perfectly follow the variation of G. To validate our ANN-MPPT, we compared it (in Figure 12) with one of the most popular MPPT algorithms, the P&O-MPPT algorithm, presented in [20–22] and [23]. It is noted that the maximum power ($P_{pv\_max} = P_{PVG\_max} = 1066$ W) as well as the maximum current are obtained when the irradiance (G) is maximum (at noon). For high values of G (thus high P_{pv}), the results of the two algorithms MPPTs are similar. We are not attempting to understand the slight difference between the two MPPTs for low values of G as this is not an objective of this study, which is more oriented towards optimizing battery control. However, looking at Figure 12, both algorithms reach the maximum power

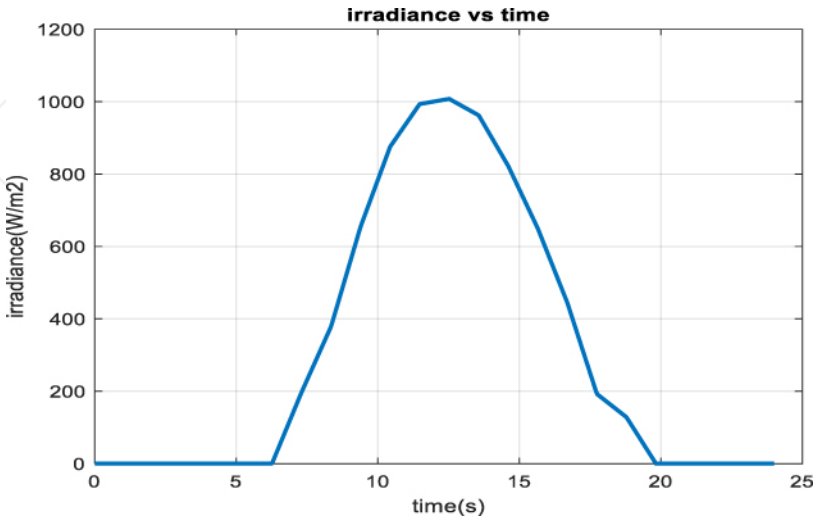

Figure 11. Daly irradiance profile [19].

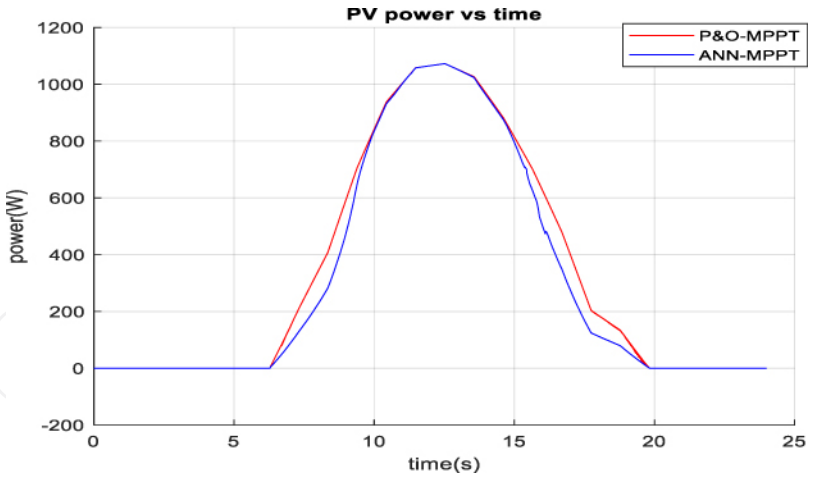

Figure 12. PV power variation.

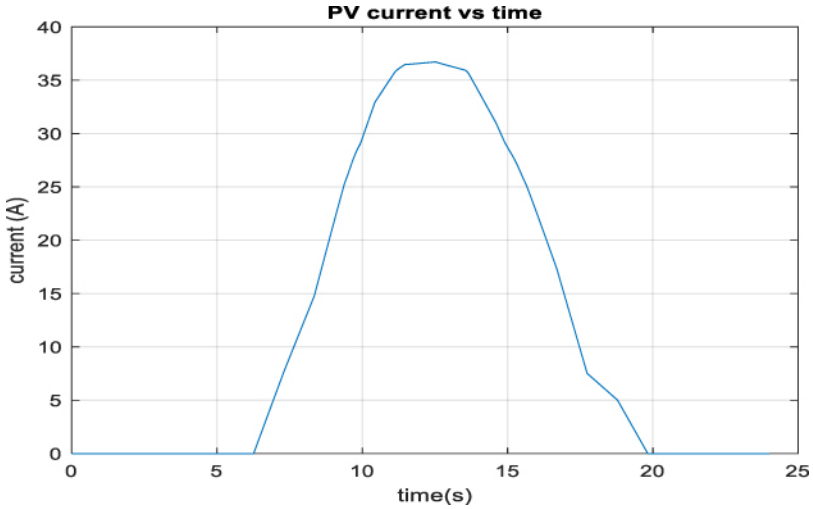

Figure 13. Variation of PV current.

point (MPP). This means that the developed ANN-based MPPT algorithm worked and can be validated.

Figure 15 shows the battery current variation (I_{bat}) when the battery is controlled with an ANN-LM control. It can be seen in Figure 15 that I_{bat} is complementary to I_{pv} (Figure 13 vs Figure 15). This means that in the presence of a sufficient irradiance (G) (during day), the PVG supplies the DC load and charges the battery at the same time. This situation results in an increase in SoC (Cf. Figure 14) and a negative I_{bat} (Cf. Figure 15). Figure 15 also shows that the maximum battery charging current is reached at noon ($I_{bat\_max} = -8.88$ A). When it discharges (SoC decreases and I_{bat} increases), the battery powers the DC load (when G is low).

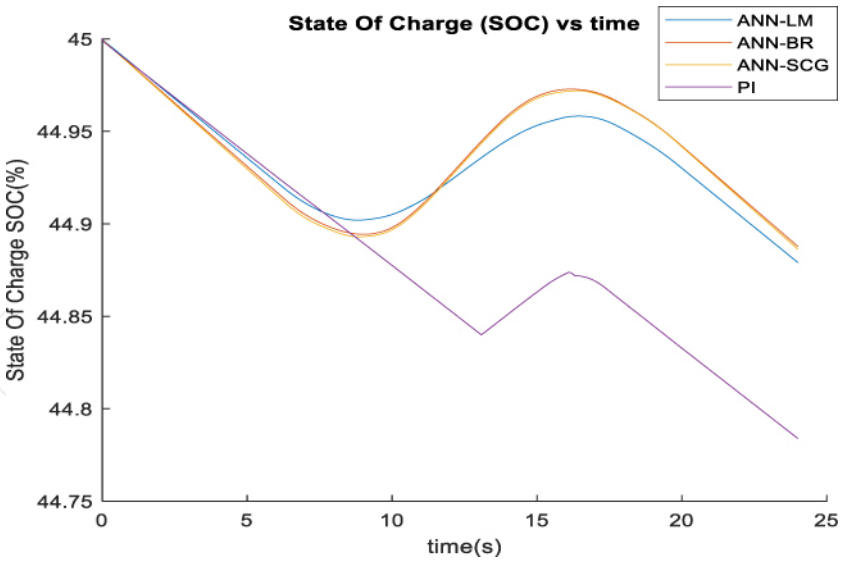

Figure 14. State of Charge (SoC).

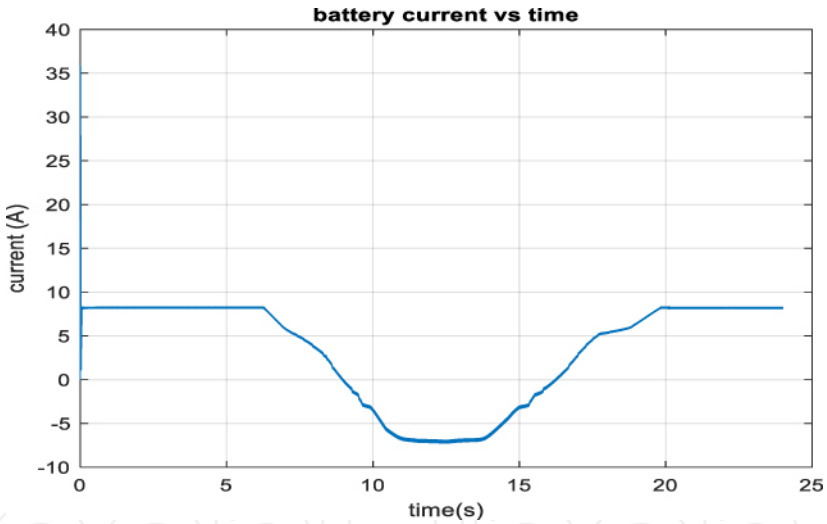

Figure 15. Battery current variation (with ANN-LM control).

Figure 14 and Figure 16 show the comparison of all our control methods described in the previous section (ANN-LM, ANN-BR, ANN-SCG and PI). To make this comparison, we have superposed the battery SoC as well as the variations of the battery current (I_{bat}) curves.

Figure 14 shows that the PI control discharges the battery more quickly and deeply than the ANN control (ANN-LM, ANN-BR, ANN-SCG). But in terms of charge, it's the opposite. The battery controlled by an ANN controller charges more than if it was controlled by a conventional PI controller. It can also be that in discharge mode, the PI control presents some oscillations which are probably be due

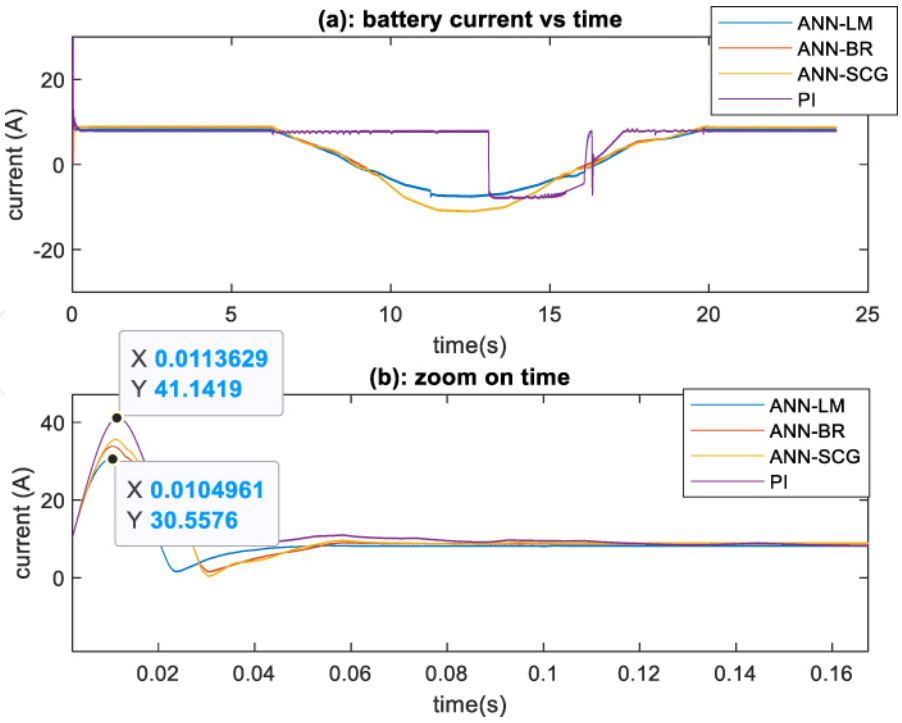

Figure 16. Superposition of I_{bat} curves: ANNs vs PI.

to an instability. It should also be noted that the charge and discharge are progressive in the case of an ANN control while they are brutal in the case of a PI control. So, it can be concluded that ANN control is better than conventional PI control because the battery does not display brutal charge-discharge and deep discharge.

Still Figure 14 shows that the results of the two controllers ANN-BR and ANN-SCG are similar. Indeed, their curves are almost merged. It can also be seen that these two controllers (ANN-BR and ANN-SCG) allow faster charging than the ANN-LM controller. But the ANN-LM controller presents the best compromise of charging and discharging speed. Moreover, we must choose the controller that stresses the battery the least. Therefore, the ANN-LM controller is better in terms of fixed objective than the ANN-BR and ANN-SCG controllers.

Figure 16 indicates that the battery current variation is progressive in the case of the ANN control (ANN-LM , ANN-BR and ANN-SCG) while it is brutal in the case of the PI control (Cf. Figure 16a). We can also observe good behavior of system transients in the case of an ANN control, which is very interesting insofar as the battery is less stressed with an ANN control and consequently it contributes to extending its lifetime. Moreover, Figure 16a shows that the battery charging time is very limited in the case of a PI control. This means that the battery continues to supply the DC load despite the presence of G. Therefore, it can be inferred that the PI control is not optimal, so not intelligent. We can also notice in Figure 16a that the

two ANN controllers (ANN-BR and ANN-SCG) show similar results. Their curves exceed the maximum current expected for our application (−11.069 A instead of −8.88 A) unlike the ANN-LM controller which respects this amplitude.

Still with the objective of comparing the performance of the four controllers (ANN-LM, ANN-BR, ANN-SCG and PI), we zoomed in on the transient regimes at the start of the simulation. This situation is shown in Figure 16b. We notice that the current overshoot (current peak) in transient regimes is more important in the case of the PI control than in the worst case of the ANN control (ANN-SCG). Indeed, we note in Figure 16b that in terms of current overshoot in transient regimes, PI control is worse than ANN-SCG control, ANN-SCG control is worse than ANN-BR control and ANN-BR is worse than ANN-LM control. So again, the best controller (the best algorithm) is the ANN-LM controller. In the case where the system is controlled with an PI control, the current peak in transient regimes at the start of the simulation is equal to 41.14 A. This current peak is reduced to 30.56 A in the best case of the ANN control (ANN-LM) i.e., a reduction of 26%. We can therefore conclude that the ANN-LM control improves the performance of the system in transient regimes, it does not stress the battery too much, it respects the technological constraints of the battery and thus improves its lifetime. This is relevant in the context of French Guiana where the equipment is not designed to be used in a severe tropical climate and therefore deteriorates rapidly.

4. Conclusion

The main purpose of this study was to design an optimal control to better control the PV-Battery microgrid to be used in the context of use in French Guiana to help improve battery lifetime.

For this, an ANN-based MPPT algorithm was first designed and applied for PV source control. The simulation result showed that the developed ANN-based MPPT algorithm worked well.

Then, to control the battery, two configurations (method1 and method2) of the ANN controller based on the feed-forward backpropagation neural network (FFBNN) associated with a Levenberg–Marquardt (LM) algorithm were designed. For each configuration, an optimal number of hidden layers was obtained. The comparison between method1 and method2 made it possible to identify the best configuration (method1) which was retained in this work.

Then, to compare the LM algorithm with other algorithms, the same model trained with the LM algorithm was tested (under the same conditions) with two other algorithms: Bayesian regularization (BR) and scaled conjugate gradient (SCG) methods. Finally, a comparison was made between the different ANN controls on

the one hand and between the best ANN control and the conventional PI control on the other hand. Regarding the comparison between the three ANN controllers (ANN-LM, ANN-BR and ANN-SCG), it was shown that the two controllers (ANN-BR and ANN-SCG) are almost similar and that the best ANN controller is the ANN-LM controller which better improved the performance in transient regimes. This ANN-LM controller also allowed a reduction in peak current of 26% compared to conventional PI control.

Moreover, the ANN-LM control allowed optimal control of the battery. It improved transient regimes to better respect the technological constraints of the battery and thus extend its lifetime. This therefore reduced the overall operating cost of the system.

Conflict of interest

The authors declare no conflict of interest.

References

1 Alvarez G, Moradi H, Smith M, Zilouchian A. *Modeling a Grid-Connected PV/Battery Microgrid System with MPPT Controller, Washington, DC, USA: IEEE 44th Photovoltaic Specialist Conference (PVSC)*. Piscataway, NJ: IEEE; June 2017. doi:10.1109/PVSC.2017.8366738.

2 Ammari C, Belatrache D, Touhami B, Makhlouf S. Sizing, optimization, control and energy management of hybrid renewable. *Energy Built Environ*. 2022;**3**: 399–411.

3 Li Z, Ma T. Distributed photovoltaics with peer-to-peer electricity trading. *Energy Built Environ*. October 2022;**3**(4):424–432.

4 Sahri Y, Tamalouzt S, Belaid SL, Bajaj M, Ghoneim SSM, Zawbaa HM, et al. Performance improvement of Hybrid System based DFIG-Wind/PV/Batteries connected to DC and AC grid by applying Intelligent Control. *Energy Rep*. 2023;**9**: 2027–2043.

5 Mehrasa M, Amirkhan S, Souraki HP, Ahmadigorji M. A robust control strategy for power management of a DC microgrid based on EVs in presence of energy storage battery. *Electr Power Syst Res*. 2023;**219**: 109229.

6 ADEME. Vers l'autonomie énergétique en zone non interconnectée (ZNI) en Guyane, Cayenne [Internet]; 2020. Available from: https://guyane.ademe.fr/expertises/energies-renouvelables/lautonomie-energetique-en-guyane.

7 M. écologique. Programmation Pluriannuelle de l'Energie (PPE) 2016–2018 et 2019–2023 de la Guyane [Internet]; 2017. Available from: https://www.ecologie.gouv.fr/sites/default/files/PPE%20Guyane%20-%20Rapport.pdf.

8 Nor AFM, Salimin S, Abdullah MN, Ismail MN. Application of artificial neural network in sizing a stand-alone photovoltaic system: a review. *Int J Power Electron Drive Syst (IJPEDS)*. Mar 2020;**11**(1):342–349. ISSN: 2088-8694. doi:10.11591/ijpeds.v11.i1.

9 Olabi AG, Abdelkareem MA, Semeraro C, Al Radi M, Rezk, O.Muhaisen H, Al-Isawi OA, Sayed ET. Artificial neural networks applications in partially shaded PV systems. *Therm Sci Eng Prog*. 2023;**37**: 101612.

10 Ben Cheikh O, Biteur Y. Étude et réalisation d'un système de poursuite du point de puissance maximale en utilisant les réseaux de neurones artificiels - Application au système photovoltaïque [thesis]. Universite Kasdi Merbah Ouargla; June 2018.

11 Charroufa O, Betkaa A, Abdeddaima S, Ghamrib A. Artificial Neural Network power manager for hybrid PV-wind desalination system. *Math Comput Simul [Internet]*. 2020;**167**: 443–460. Available from: www.sciencedirect.com.

12 Raja Sekhar Reddy B, Veera Reddy VC, Vijaya Kumar M. Modelling and analysis of DC-DC converters with AI based MPP tracking approaches for grid-tied PV-fuel cell system. *Electr Power Syst Res*. 2023;**216**: 109053.

13 Aallouche A, Ouadi H. Online fault detection and identification for an isolated PV system using ANN. *IFAC-PapersOnLine*. 2022;**55**(12):468–475. ISSN 2405-8963, doi:10.1016/j.ifacol.2022.07.356.

14 Baojie L, Delpha C, Diallo D, Migan-Dubois A. Application of artificial neural networks to photovoltaic fault detection and diagnosis: A review. *Renew Sustain Energy Rev*. 2020;**138**: 110512. doi:10.1016/j.rser.2020.110512. hal-03087601.

15 Kaushal J, Basak P. Power quality control based on voltage sag/swell, unbalancing, frequency, THD and power factor using artificial neural network in PV integrated AC microgrid. *Sustain Energy Grids Netw*. 2020;**23**: 100365.

16 Sedaghati F, Nahavandi A, Badamchizadeh MA, Ghaemi S, Fallah MA. PV Maximum power-point tracking by using artificial neural network. *Math Probl Eng*. 2012;**2012**: 506709. p. 10.

17 L solution. MATLAB implementation of neural network based MPPT for solar PV system [Internet]. YouTube; 2020. Available from: https://www.youtube.com/watch?v=WgZgjSkv69Y.

18 Mahamat C, Ilunga G, Bechet J, Zermani S, Linguet L. Artificial neural network in photovoltaic-battery microgrid system for controlling the battery current in French Guiana: battery life improvement. In: *2022 13th International Renewable Energy Congress (IREC)*. Piscataway, NJ: IEEE; 2022. p. 1–6. doi:10.1109/IREC56325.2022.10002124.

19 Bechet J, Albarelo T, Macaire J, Salloum M, Zermani S, Primerose A, et al. Updated GOES-13 Heliosat-2 method for global horizontal irradiation in the Americas. *Remote Sens*. 2022;**14**(1):224. doi:10.3390/rs14010224.

20 Subramanyam PV, Vyjayanthi C. Integration of PV and battery system to the grid with power quality improvement features using bidirectional AC-DC converter. In: *2016 International Conference on Electrical Power and Energy Systems (ICEPES), Maulana Azad National Institute of Technology, Bhopal, India*. Piscataway, NJ: IEEE; Dec 14–16 2016.

21 Sopian K, Elbreki AM, Ruslan MH, Al-Shamani AN, Elhub B, Abed AM, Hasan HA, Dezfouli MMS. *A stand-alone Photovoltaic System Design and Sizing: a Greenhouse Application in Sabha City: Case study in Libya, Padang Indonesia: Proceeding of The 3rd Engineering Science And Technology? International Conference (ESTIC)*, vol. 3, 2016. ISSN 2548 8902.

22 Motahhir S, El Ghzizal A, Derouich A. Modélisation et commande d'un panneau photovoltaïque dans l'environnement PSIM, fès: Congrès International de Génie Industriel et Management des Systèmes; May 2015, fès, Maroc. ffhal-01351493f.

23 Nkambule MS, Hasan AN, Ali A. MPPT under partial shading conditions based on Perturb & Observe and Incremental Conductance, 2019 11th International Conference on Electrical and Electronics Engineering (ELECO) [Internet]; 2019. https://www.researchgate.net/figure/Soltech-1STH-215-P-PV-Panel-and-Boost-DC-DC-converter-specifications_tbl1_339261887 doi:10.23919/ELECO47770.2019.8990426.